UNIVERSITY OF STOCKHOLM

INSTITUTE OF PHYSICS

HIGGS BOSON EVENTS AND BACKGROUND AT LEP

A MONTE CARLO STUDY

G. EKSPONG and K. HULTQVIST

USIP Report 82 - 05 June 1982

USIP -- 82 -05

HIGGS BOSON EVENTS AND BACKGROUND AT LEP

A Monte Carlo Study

G. Ekspong and K. Hultqvist

Department of Physics, University of Stockholm
Vanadisvägen 9, S-113 46 Stockholm

ABSTRACT

Higgs boson production at LEP using $e^+e^- \to Z^0 \to H^0 + e^+e^-$ has been studied by Monte Carlo generation of events with realistic errors of measurement added.

The results show the recoil mass (Higgs boson mass) resolution to be reasonably good for boson masses $\gtrsim 5$ GeV.

The events are found to populate a phase space region free of physical background for all boson masses below about 35 GeV. For masses above 40 GeV the Higgs boson signal merges with the physical background produced by semi-leptonic decays of heavy flavour quarks while diminishing in strength to low levels.

The geometrical acceptance of a detector like DELPHI is about 80% for Higgs boson events.

1. INTRODUCTION

In the standard electroweak theory (Ref. 1) spontaneous symmetry breaking is achieved by the Higgs mechanism. One neutral Higgs boson with known couplings appears in the theory as a challenge for experimental researchers. Its mass has not been predicted. Methods which cover as wide a range in mass as possible are therefore valuable.

It has been pointed out (Ref. 2) that the reaction

$$e^+e^- \rightarrow Z^0 \rightarrow H^0 + \ell^+ + \ell^- \qquad \text{(i)}$$

is quite favourable for not too heavy Higgs bosons (H^0). The signature in an event for reaction (i) is two fast leptons (e:s or μ:s) with high invariant mass and many particles arising in the decay of the Higgs boson.

The method would be to look for a peak in the missing mass recoiling against the two fast leptons, and after finding it to look into the detailed composition of the decay products. In the absence of errors and background the recoil mass would be equal to the Higgs boson mass.

We have applied Monte Carlo methods for simulating events according to reaction (i) and to add realistic errors of measurement to the observed tracks. In this way the mass resolution for various assumed boson masses has been obtained and also the expected geometrical acceptance of a proposed detector (DELPHI, Ref. 3, Fig. 1)

The physical background from the semi-leptonic decays of heavy quarks produced by $Z^0 \rightarrow q\bar{q}$, has also been studied by us in great detail using Monte Carlo methods. A scatterplot of recoil mass versus invariant dilepton mass in each event is very useful for separating the signal (Higgs boson events) from the background.

Studies of these or similar questions have been carried out earlier (Ref:s 4 & 5). The results of Ref. 4 is, however, at variance with ours in that we find a better mass resolution for the recoil mass and a different range of detectable boson masses. Our methods of analysis and of background simulation are different and more detailed.

2. FUNDAMENTAL RELATIONS

Finjord (Ref. 6) gives the following expression for the differential rate for $Z^0 \to H^0 + e^+ e^-$.

$$\frac{d\Gamma}{d\varkappa^2} = \frac{G_F^2 M_Z^5 (c_L^2 + c_R^2)}{192\pi^3((\varkappa^2 - 1 - \frac{1}{4}\Delta^2)^2 + \Delta^2)} \lambda^{\frac{1}{2}}(1, \mu^2, \varkappa^2)(2\varkappa^2 + \frac{1}{6}\lambda(1, \mu^2, \varkappa^2)) \qquad \text{(ii)}$$

In this formula $\varkappa = M_{e^+e^-}/M_Z$, where $M_{e^+e^-}$ is the effective mass of the e^+e^--pair. Δ is the relative width of Z^0 and $\mu = M_H/M_Z$ is the relative mass of the Higgs boson. The scale factor

$$\frac{G_F^2 M_Z^5 (c_L^2 + c_R^2)}{192\pi^3}$$

varies with $\sin^2\theta_W$.

Integration of (ii) yields the total rate. As can be seen from Fig. 2 this drops rapidly with increasing M_H (Ref. 6).

If p, k, p' and k' are the four-momenta of the incoming and outgoing e^- and e^+, respectively, then, neglecting V-A interference, the matrix element squared contains the factor

$$|M|^2 \propto [(pk')(p'k) + (pp')(kk')] \quad . \qquad \text{(iii)}$$

(Ref. 7)

This gives a total differential rate

$$\frac{d^5\Gamma}{d\varkappa^2 d(\cos\theta)d\varphi d(\cos\theta_{eH})d\varphi_{eH}} = \frac{G_F^2 M_Z^5 (c_L^2 - c_R^2)\varkappa^2\lambda^{\frac{1}{2}}(1,\mu^2,\varkappa^2)}{2^{11}\pi^5[(\varkappa^2 - 1 + \frac{1}{4}\Delta^2)^2 + \Delta^2]} \cdot \{\gamma^2[1 + \cos^2\theta\cos^2\theta_{eH}$$

$$+ 2\gamma\cos\theta\sin\theta\cos\theta_{eH}\sin\theta_{eH}\cos\varphi_{eH} + \sin^2\theta\sin^2\theta_{eH}\cos^2\varphi_{eH} - \gamma^2\beta^2(\cos^2\theta + \cos^2\theta_{eH})] \qquad \text{(iv)}$$

where β and γ are the velocity and Lorentz-factor, respectively, for the e^+e^--pair in CMS. The angles are defined in Fig.3. Formula (ii) can be rederived by integrating over the angles.

3. RATES

The cross section for $e^+e^- \rightarrow Z^0 \rightarrow$ visible states (excluding $\nu\bar{\nu}$ and Bhabas) at the energy of the Z^0 peak is (Ref. 8):

$$\sigma(e^+e^- \rightarrow Z^0_{vis}) = 2600\,\sigma_{pt} \qquad (v)$$

where σ_{pt} is the point-like QED cross section. For $\sqrt{s} = 90$ GeV $= M_Z$ this is

$$\sigma_{pt} = 10.7 \text{ pb} .$$

Assuming a luminosity of $6 \cdot 10^{30}$ $s^{-1}cm^{-2}$, one year's running (2500 h) gives an integrated luminosity of 54 pb^{-1}, or

$$1.5 \cdot 10^6 \; Z^0/\text{yr} .$$

Using $B(Z^0 \rightarrow e^+e^-) = 3.71\%$ (for the visible Z^0:s) one obtains the following average number of reactions of type (i) in a one year run:

Table 1

Higgs boson mass (GeV)	5	10	15	20	25	30	40
n:o of events	223	127	79	51	33	22	9

4. THE MONTE CARLO GENERATION OF EVENTS

We generated the events according to formula (iv), using $M_Z = 90$ GeV with a width of 3 GeV.

Because of the axial symmetry the φ dependence is trivial, φ beeing uniformly distributed between 0 and 2π.

The remaining four-dimensional generation problem was reduced to four successive one-dimensional ones. This was done by keeping the variables already generated fixed, while integrating out the ones not yet to be generated, thus obtaining a conditional and marginal distribution in the wanted variable, x. The distribution obtained, dN/dx, was normalized to one:

$$\int_{-\infty}^{\infty} \frac{dN}{dx}\, dx = 1$$

Generating a random number, ξ, uniformly distributed between 0 and 1 and choosing x to fulfil

$$N(x) = \int_{-\infty}^{x} \frac{dN}{dx}\, dx = \xi \qquad \text{(vi)}$$

gives x-values with the desired distribution.

The first variable we generated was $\varkappa (= M_{e^+e^-}/M_Z)$. Integrating over all angles gives the cumulative distribution

$$N(\varkappa) = \frac{\int_0^{\varkappa} d\Gamma/d\varkappa^2\, 2\varkappa d\varkappa}{\int_0^{1-\mu} d\Gamma/d\varkappa^2\, 2\varkappa d\varkappa} \qquad \text{(vii)}$$

where $d\Gamma/d\varkappa^2$ is given in formula (ii). For each Higgs boson mass $N(\varkappa)$ was calculated numerically for 300 values of $\varkappa$. For each event a ξ was generated and equation (vi), $N(\varkappa) = \xi$, was solved for $\varkappa$ by linear interpolation.

With $\varkappa$ fixed to this value $\cos\theta_{eH}$ was generated according to the same principle. Integrating over φ_{eH} and $\cos\theta$ and normalizing one obtains the distribution

$$\frac{dN}{d(\cos\theta_{eH})} = A_+ + A_- \cos^2\theta_{eH}$$

where

$$A_\pm = \frac{3(1 \pm \gamma^2)}{4(2 + \gamma^2)}$$

Equation (vi) now reads :

$$\cos^3\theta_{eH} + \frac{3A_+}{A_-}\cos\theta_{eH} + \frac{3}{A_-}(A_+ - \xi) + 1 = 0 \qquad \text{(viii)}$$

This third degree polynomial equation in $\cos\theta_{eH}$ was solved algebraically.

Keeping $\varkappa$ and $\cos\theta_{eH}$ fixed gives a similar expression for $\cos\theta$:

$$\frac{dN}{d(\cos\theta)} = A_+ + A_- \cos^2\theta$$

This time, however,

$$A_\pm = \frac{3(\cos^2\theta_{eH} + 1 \pm 2\gamma^2(1-\cos^2\theta_{eH}))}{8(\cos^2\theta_{eH} + 1 + \gamma^2(1-\cos^2\theta_{eH}))}$$

The resulting equation for $\cos\theta$ is the same as (viii) for $\cos\theta_{eH}$ and was solved in the same way.

Keeping $\varkappa, \cos\theta_{eH}$ and $\cos\theta$ fixed the cumulative distribution in φ_{eH} is

$$N(\varphi_{eH}) = U\varphi_{eH} + V\sin\varphi_{eH} + W\sin 2\varphi_{eH} \qquad \text{(ix)}$$

where $U = \frac{1}{2\pi}$

$$V = \frac{1}{\pi N_{eH}} 2\gamma\cos\theta_{eH}\sin\theta_{eH}\cos\theta\sin\theta$$

$$W = \frac{1}{4\pi N_{eH}} \sin^2\theta_{eH}\sin^2\theta$$

$$N = 2\left[\gamma^2 + \gamma^2\cos^2\theta_{eH}\cos^2\theta - (\gamma^2-1)(\cos^2\theta_{eH} + \cos^2\theta)\right] + \sin^2\theta_{eH}\sin^2\theta$$

Equation (vi) $\qquad N(\varphi_{eH}) = \xi$,
was now solved numerically.

Finally a Lorentz boost and a rotation yields the four-momentum of the electron in CMS (with the z-axis parallel to the beam):

$$p_Z = \frac{\varkappa}{2} M_Z \left[\gamma(\cos\theta_{eH} - \beta)\cos\theta + \sin\theta_{eH}\cos\varphi_{eH}\sin\theta\right]$$

$$p_X = \frac{\varkappa}{2} M_Z \left[\gamma(\cos\theta_{eH} - \beta)\sin\theta\cos\varphi - (\cos\theta\cos\varphi\cos\varphi_{eH} - \sin\varphi\sin\varphi_{eH})\sin\theta_{eH}\right]$$

$$p_Y = \frac{\varkappa}{2} M_Z \left[\gamma(\cos\theta_{eH} - \beta)\sin\theta\sin\varphi - (\cos\theta\sin\varphi\cos\varphi_{eH} + \cos\varphi\sin\varphi_{eH})\sin\theta_{eH}\right]$$

$$E = \frac{\varkappa}{2} M_Z \left[1 - \beta\cos\theta_{eH}\right] \qquad \text{(x)}$$

The positron momentum is obtained by the transformation

$$\theta_{eH} \rightarrow \pi - \theta_{eH}$$

$$\varphi_{eH} \rightarrow \pi + \varphi_{eH}$$

5. PROCESSING OF THE GENERATED EVENTS

We studied the detection of the generated events in the DELPHI detector. All events with both electron and positron passing through an electromagnetic calorimeter were accepted.

The acceptance was found to be 80%, and is independent of M_H (see Fig. 4). The barrel calorimeter accepts about 50% of the events and the end cap calorimeter adds about 30%, either alone or in combination with the barrel.

Normally distributed errors were added to the energies with

$$\frac{\Delta E}{\sqrt{E}} = \begin{cases} 0.10 & \text{forward calorimeter} \\ 0.11 & \text{barrel calorimeter} \end{cases}$$

We also added errors to the angles using $\Delta\theta = \Delta\varphi = 0.4$ mrad for tracks passing through the forward chambers and $\Delta\theta = \Delta\varphi = 1.5$ mrad elsewhere. The errors in energy are the dominating ones.

6. SINGLE PARTICLE DISTRIBUTIONS

The single-electron energy spectrum for $M_H = 10$ GeV is shown in Fig. 5. It is peaked at high energies (~ 40 GeV). The electromagnetic calorimeters in DELPHI give a good measurement of these high electron energies. For muons the situation is different, and for energies above 15 GeV the precision is better for electrons. This is the reason for using the reaction $Z^0 \rightarrow H^0 e^+ e^-$, rather than $Z^0 \rightarrow H^0 \mu^+ \mu^-$.

The electron angular distribution has a $(1 + A\cos^2\theta)$ shape (Ref. 9), as can be seen from Fig. 6, showing also the acceptance of the calorimeters. The main loss of events is caused by the gap between the end-cap and the barrel.

7. SEARCH FOR HIGGS BOSONS

The effective mass of the e^+e^--pair and the recoil mass (= boson mass) were calculated (setting the electron mass to 0):

$$M^2_{e^+e^-} = 2(E_{e^+}E_{e^-} - \mathbf{P}_{e^+} \cdot \mathbf{P}_{e^-})$$

$$M^2_{recoil} = s + M^2_{e^+e^-} - 2\sqrt{s}\,(E_{e^+} + E_{e^-}) \qquad \text{(xi)}$$

Figs 7 and 8 are scatter plots of M_{recoil} vs $M_{e^+e^-}$ for M_H = 10 GeV and 30 GeV, respectively. The spread in recoil mass is caused by measurement errors, whereas that in electron pair mass is due mainly to the physical variation of $\varkappa$. As can be seen from the plots, and also from Fig. 9, this distribution is strongly peaked towards high effective masses, i.e. the e^+ and e^- tend to be back to back and of high energies (Fig. 5). The maximum value of $M_{e^+e^-}$, however, is $M_Z - M_H$ and therefore the points move towards the upper left-hand corner of the plot with increasing M_H.

The spread in recoil mass is reasonably small and decreases with increasing M_H. This can be seen from Figs 7 and 8 or 10 and 11 (showing histograms of M_{recoil}). The width, as obtained in generated Monte Carlo samples of 2 000 events of which ~1 600 were accepted by the detector, is shown in the table below.

Table 2

Higgs boson mass (GeV)	5	10	20	30
Recoil mass spread (GeV)	4.4	2.5	1.8	1.5

These widths have been obtained by dividing the standard deviation of the recoil mass squared by twice the recoil mass. This was done to avoid the problem of skew distributions and negative values of the squared recoil mass for low Higgs boson masses.

For values of M_H smaller than about 5 GeV the mass resolution deteriorates, but the higher rate expected at low M_H compensates to some degree for the larger spread. The presence of a signal should be clear even at low masses.

For large M_H the rate drops, giving an upper limit for the Higgs boson to be detectable. This limit depends on the LEP luminosity and the running time. As will be seen below background events also impose a limit.

The relatively small spread in recoil mass and the characteristic distribution in electron pair mass provide a good signal which is comparatively free of background for all Higgs boson masses below about 35 GeV as will be seen below.

8. BACKGROUND

The Lund Monte Carlo programme (Ref. 10) was used to examine the effect of background due to semi-leptonic decay of heavy quarks (q) formed by the process

$$e^+e^- \rightarrow Z^0 \rightarrow q\bar{q}$$

The Z^0 branching ratios are (Ref. 11)

$$\nu\bar{\nu} : \ell^+\ell^- : q_{2/3}\bar{q}_{-2/3} : q_{-1/3}\bar{q}_{1/3} = 2 : 1.04 : 3.63 : 4.67$$

Events of the types $Z^0 \rightarrow c\bar{c}$, $b\bar{b}$, $t\bar{t}$ with or without hard gluons were generated in the expected proportions. The total Monte Carlo sample consists of 390 000 events which corresponds to an integrated luminosity of 33 pb^{-1} or a run of $5.5 \cdot 10^6$ s at a luminosity of $6 \cdot 10^{30}$ cm^{-2} s^{-1}.

The mass of the t quark is taken as about 20 GeV. The results should, however, not critically depend on the assumed t quark mass, since the separately studied $b\bar{b}$ sample gives similar results in our scatterplots. A heavy quark in a meson undergoes a fast decay chain and electrons (or positrons) will be produced in semi-leptonic decays at various points along the chain.

The branching ratios for $e^{\pm}$-decays are those used in the Lund programme, i.e. 9 and 12% for various top mesons, 11, 16 and 17% for beauty mesons and 5, 10 and 16% for charmed mesons. For the onium states branching ratios of 7% (J/ψ), 3% (Ψ) and 8% (φ_t) were applied. Another rather strong source of electrons and positrons are Dalitz decays of π^0 with a branching ratio of 1.2%.

Each event was checked for electrons and positrons disregarding those with energy less than 1 GeV. All electrons and positrons which were part of an accepted e^+e^--pair with effective mass less than 0.6 GeV were removed. This cut was made to remove Dalitz pairs, thereby reducing the combinatorial background. Of the remaining electrons and positrons all $e^{\pm}e^{-}$ combinations were given the same treatment as the Higgs boson events, i.e. errors of measurements were added and $M_{e^+e^-}$ and M_{recoil} computed.

Fig. 12 shows the result for $Z^0 \rightarrow b\bar{b}$. There are two ways of producing an e^+e^--pair :

$e^+e^- \rightarrow Z^0 \rightarrow b + \bar{b} \longrightarrow X$ (both leptons in the same jet)

$b \rightarrow c + e^-$

$c \rightarrow s + e^+$

(or the corresponding decay of $\bar{b}$)

$e^+e^- \rightarrow Z^0 \rightarrow b + \bar{b} \longrightarrow \bar{c} + e^+$ (one lepton in each jet)

$b \rightarrow c + e^-$

In the first reaction chain e^+e^--pairs are produced with masses less than the b mass. This gives rise to the band of points along the ordinate in Fig. 12. In the second reaction the electron and positron are parts of two nearly oppositely directed jets. They most frequently carry a small fraction of the jet momentum, which means a distribution in $M_{e^+e^-}$ peaked at low values but with a tail towards large $M_{e^+e^-}$. For a fixed $M_{e^+e^-}$, however, they tend to move back to back, i.e. M_{recoil} tends to be near the kinematic limit $M_{recoil} = M_Z - M_{e^+e^-}$. This gives rise to the diagonal band of points in Fig. 12. The cuts made reduce the number of points with a low e^+e^- mass, and also cut out the points in the upper left hand corner of Fig. 12.

Fig. 13 shows the total background. The 390 000 events of the type $Z^0 \rightarrow q\bar{q}$ gave rise to 27 432 e^+e^- combinations that survived the 1 GeV cut. These contained 5 955 low mass pairs, 5 038 of which were accepted. Removing the electrons and positrons which form these combinations reduces the number of combinations by 6 505 to 20 927. (Using also the low mass combinations that were not accepted would have meant a further reduction by 1 122.) Of the

20 927 the detector accepts 16 033 combinations (77°) which are the ones plotted in Fig. 13. The problem of finding a few e^+e^--combinations related to Higgs boson events against such a large background is addressed below.

Figs 14 - 17 show the total background together with the corresponding number of Higgs boson events for different boson masses. The number of generated Higgs boson events is 77, 31, 13 and 5 for boson masses of 10, 20, 30 and 40 GeV, respectively. The plots show the accepted events only. Clearly, for low Higgs boson masses the background and signal populate different regions of the scatterplot. Thus the Higgs boson events are background free for boson masses below about 35 GeV.

In Figs 17–21 are shown some marginal distributions for these plots. The Higgs boson events grow fewer and move into the background when $M_H \gtrsim 40$ GeV. Should the boson mass turn out to be in this high range, one would require a very high LEP luminosity to obtain a sufficient number of events, and a detailed study of the background would be necessary. Here the μe - events could help in establishing the background shape, free of Higgs boson events (Ref. 5).

9. IDENTIFICATION OF HIGGS BOSONS

A peak in the mass of the recoiling system produced in association with high mass e^+e^--pairs is only an indication of Higgs boson production. Further information should be extracted from the complete event, including the boson decay products.

Since the boson of the standard electroweak theory couples mainly to heavy fermions, the nature of the decay products should be established to the fullest extent possible. The amount of leptons, strange mesons, charmed mesons and beauty mesons among the decay products can be predicted for each boson mass.

A detector with efficient identification of particles in the few GeV range would therefore be very useful. DELPHI is particularly well suited for such a task.

10. CONCLUSIONS

It seems feasible to look for light Higgs bosons at LEP, using this method of analyzing high-mass electron pairs. The geometrical acceptance of a detector like DELPHI is about 80%, and independent of boson mass. If the boson mass is about 40 GeV or larger the signal will be small and dominated by background e^+e^- - pairs from heavy quark production and decay. This would necessitate a detailed study of the background. If it is less than about 5 GeV the spread in recoil mass makes a good relative determination of the mass difficult, but the presence of a Higgs boson should still be observable. To verify that a peak in the recoil mass spectrum is indeed caused by a Higgs boson one must also analyze the decay products of the boson.

ACKNOWLEDGEMENTS

Our thanks go to G. Gustafsson, (University of Lund), and L. Pape (CERN) for discussions, especially concerning the differential rate formula. T. Sjöstrand gave invaluable help in the use of the Lund Monte Carlo programme for this purpose.

REFERENCES

1. S. Weinberg, Phys. Rev. Lett. 19, 1264 (1967);
A. Salam, Proc. 8:th Nobel Symposium, Almqvist & Wiksell, Stockholm (1968);
J. Ellis et al, Nucl. Phys. B, 106, p 292 (1976).

2. J.D. Bjorken, SLAC - PUB - 1866 (1977)

3. DELPHI, A detector with lepton, photon and hadron identification.
Letter of intent for an experimental program at LEP. DELPHI 82/1 (CERN)

4. G. Barbiellini et al, DESY 79/27 (1979).

5. S.L. Olsen, University of Rochester CZF 81/2.

6. J. Finjord, Physica Scripta, 21, p 143 (1980).

7. L. Pape and G. Gustavsson, private communication.

8. F.A. Berends, R. Kleiss and S. Jadach, preprint. Instituut - Lorentz, Leiden (1982).

9. R.L. Kelly and T. Shimada, Phys. Rev. D, 23, p 1940 - 3 (1981).

10. T. Sjöstrand, LU TP 80 - 3, Department of theoretical physics, University of Lund, Sweden.

11. J. Ellis, Proc. of the LEP summer study, CERN yellow report 79-01, vol. 2, p 615.

Fig. 1

DELPHI, a proposed LEP detector. There is cylindrical, as well as backwards-forwards symmetry, and the figure shows one quarter of the cross section along the beam pipe (top). In our simulations we have used the positions of the electromagnetic calorimeters and the forward drift chambers. (Fig. from Ref. 1)

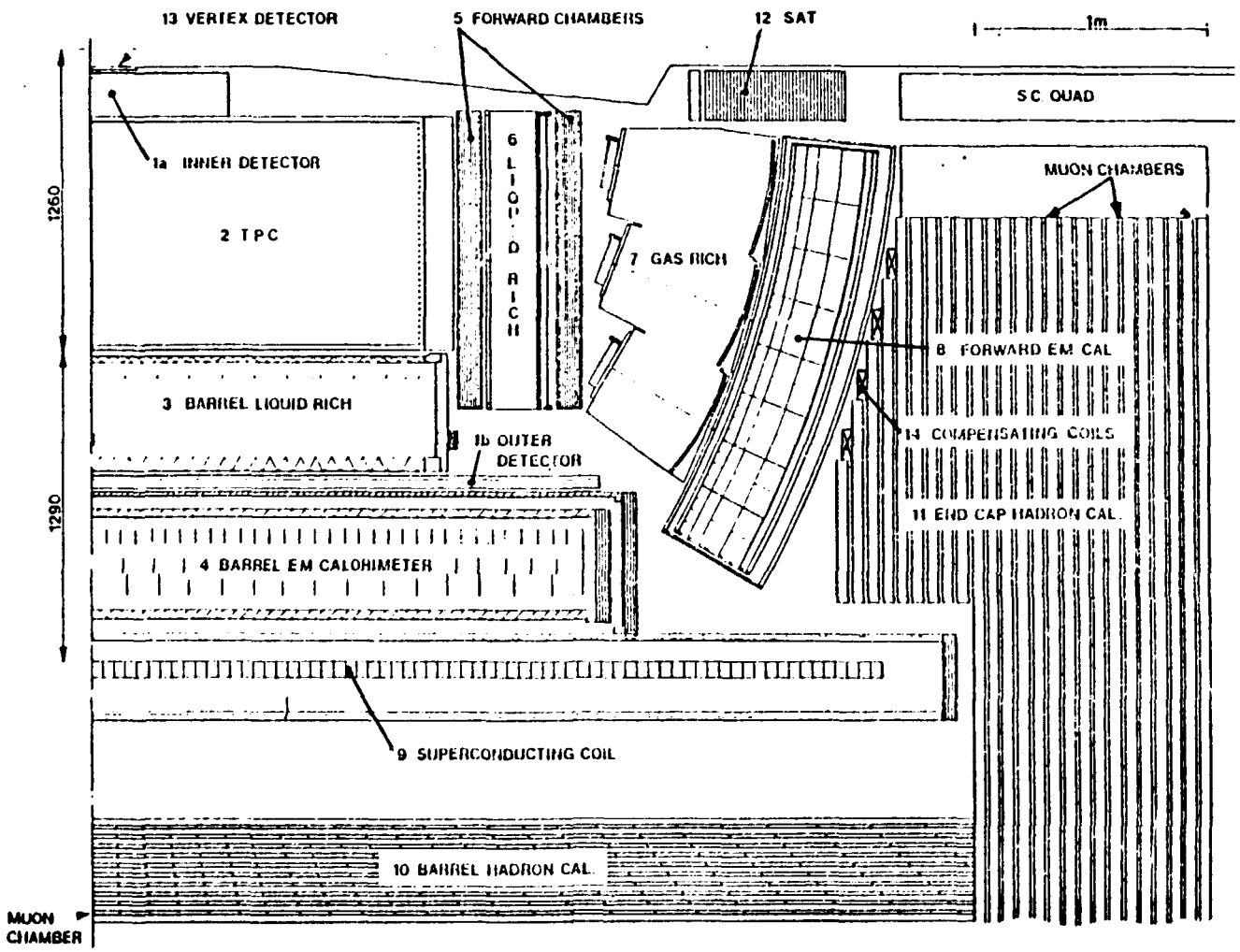

1 a. The inner detector is a drift chamber giving 12 points on each track. 1 b. The outer detector is formed of three layers of drift tubes and, together with the inner detector, is used in the trigger. 2. The 1 atm TPC gives three-dimensional space points and separates pions and electrons up to ~ 8 GeV/c by ionisation measurements. 3. The cryogenic barrel RICH counter identifies kaons up to ~ 8 GeV/c. The radiator, the photon detector and the honeycomb structure of the walls are indicated. 4. The tower structure of the liquid argon calorimeter within its cryostat is shown. 5. Forward drift chambers. 6. The warm liquid RICH counter gives π/K separation up to $\sim$ 5 GeV/c. 7. The photons produced in the gas RICH counters are focused by spherical mirrors, allowing π/K separation up to ~ 35 GeV/c. 8. The tower structure of the forward liquid argon calorimeter is similar to that of the barrel calorimeter. 9. The superconducting coil, of 2.55 m radius. 10 + 11. The tower structure of the h: iron calorimeter embedded in the iron yoke is shown. Some planes are instrumented with 4 cm cathode strips for muon identification. 12. Small angle tagger. 13. Location of the silicon microstrip vertex detector. 14. Warm compensating coils.

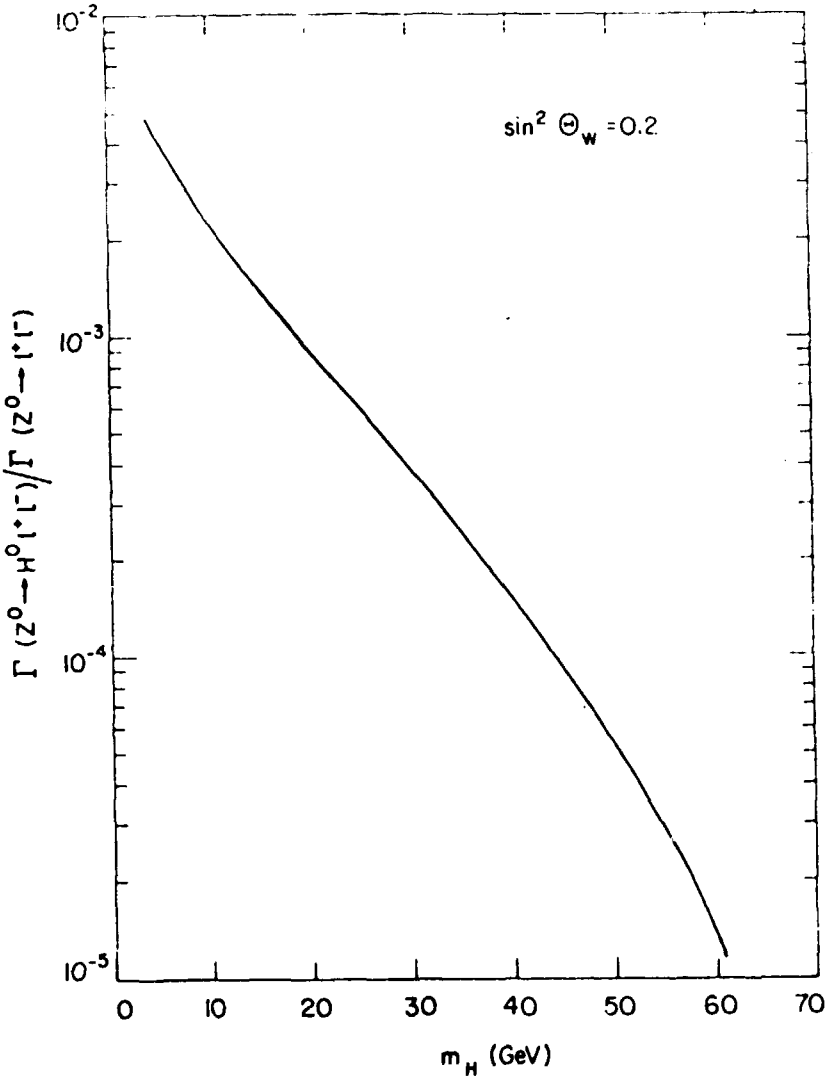

Fig. 2

The rate for the reaction $Z^0 \to H^0 e^+e^-$ normalized to the rate for $Z^0 \to \ell^+\ell^-$, the production of a (particular) lepton pair. (Fig. from Ref. 6)

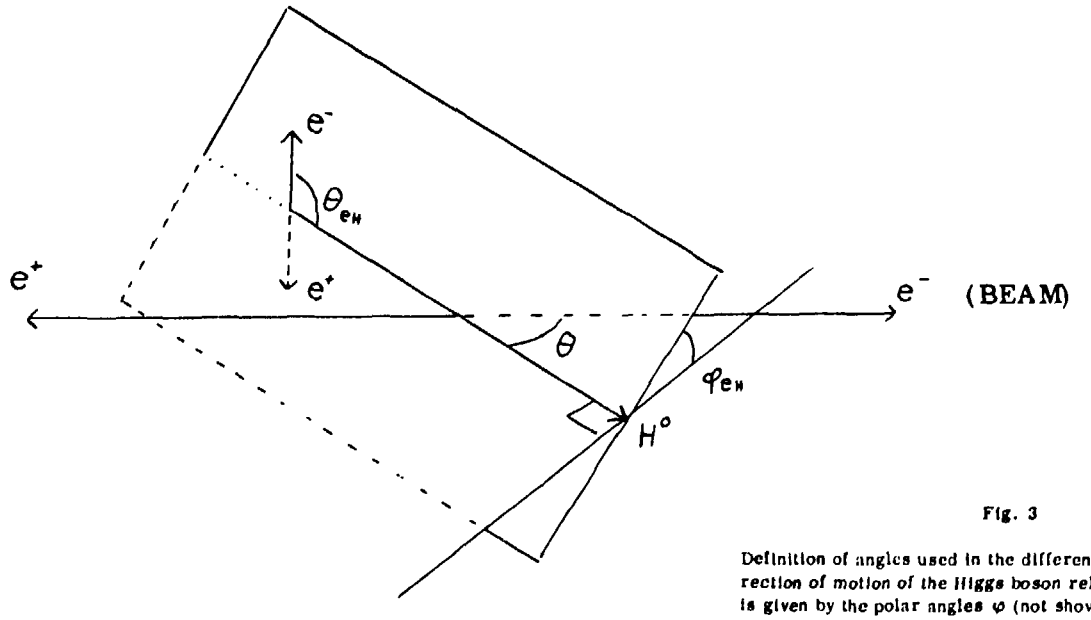

Fig. 3

Definition of angles used in the differential rate. The direction of motion of the Higgs boson relative to the beam is given by the polar angles φ (not shown) and θ. The momenta of the e^+e^--pair and that of the boson define a plane. The angle between this plane and that given by the boson momentum and the beam axis is φ_{eH}. Finally, θ_{eH} is the angle between the electron and the boson momenta in the e^+e^- rest frame.

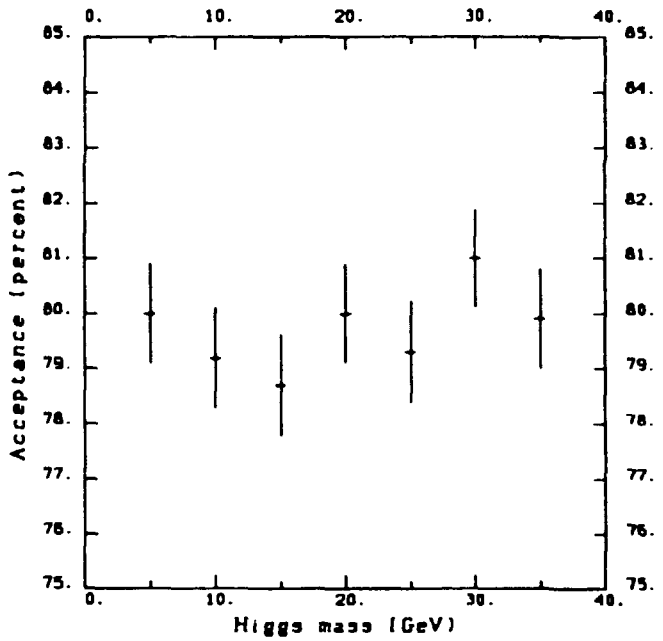

Fig. 4

The acceptance found in the Monte Carlo simulations.
It can be seen to be independent of the Higgs boson mass.

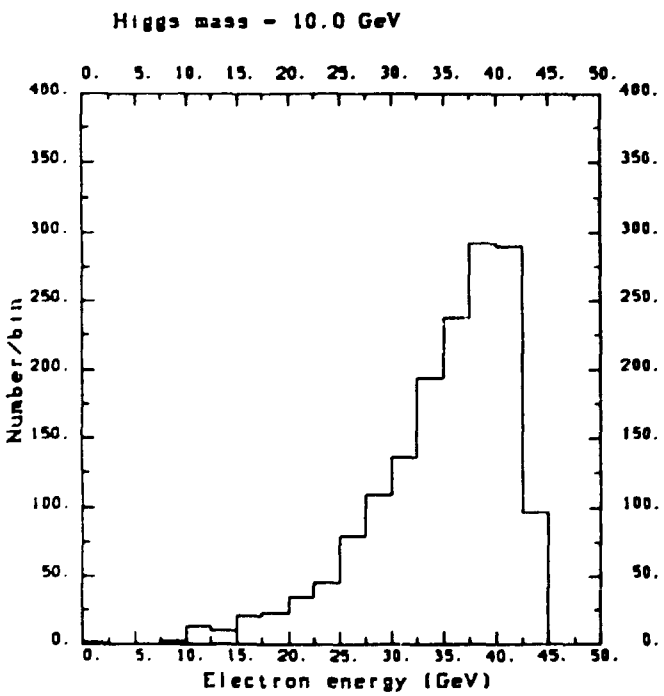

Fig. 5

Histogram of the single electron energy for M_H 10 GeV.

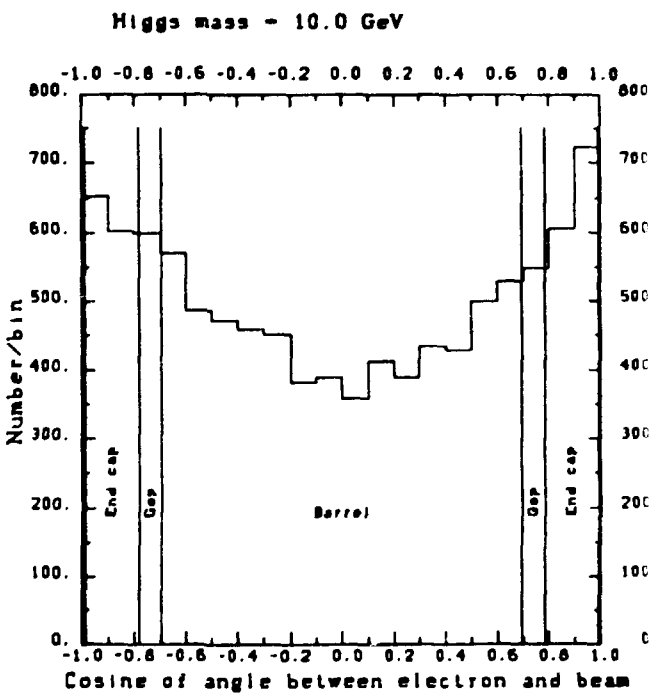

Fig. 6

The distribution of the cosine of the angle between the electron momentum and the beam axis. Also shown is the acceptance of the calorimeters. This histogram is for M_H 10 GeV. Other masses gave similar results.

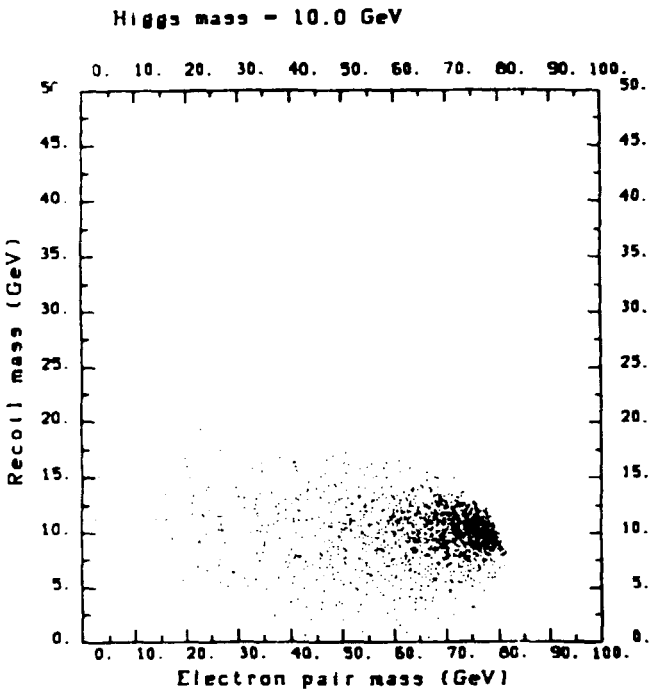

Fig. 7

Scatterplot of the recoil mass vs the e^+e^- mass for M_H = 10 GeV. Measurement errors influence the position of points. (The plot contains ~ 1 600 accepted events out of a total of 2 000.)

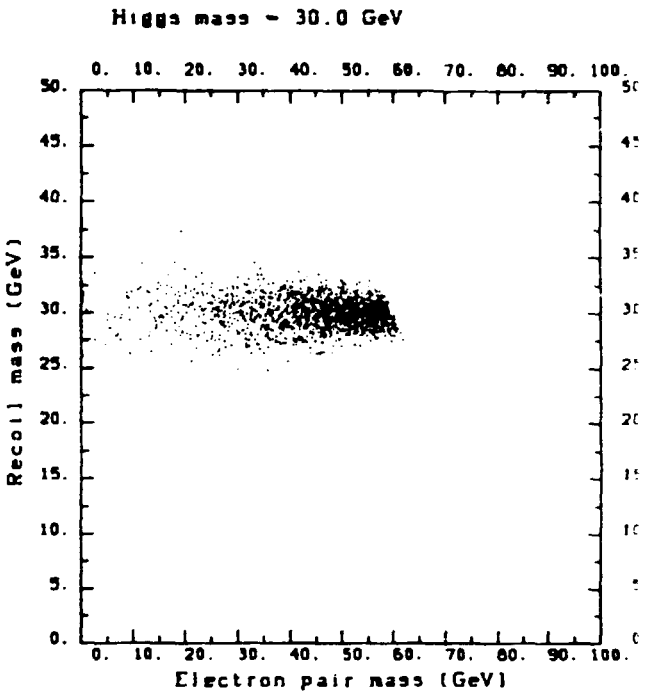

Fig. 8

Same as Fig. 7 for M_H = 30 GeV. (Number of events as in Fig. 7.)

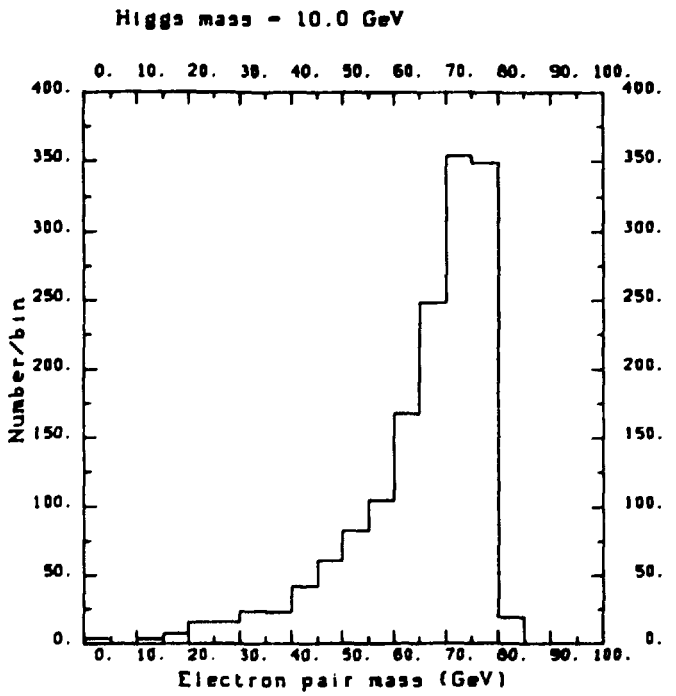

Fig. 9

Histogram of the e^+e^- mass for M_H = 10 GeV. (Same sample as in Fig. 7.)

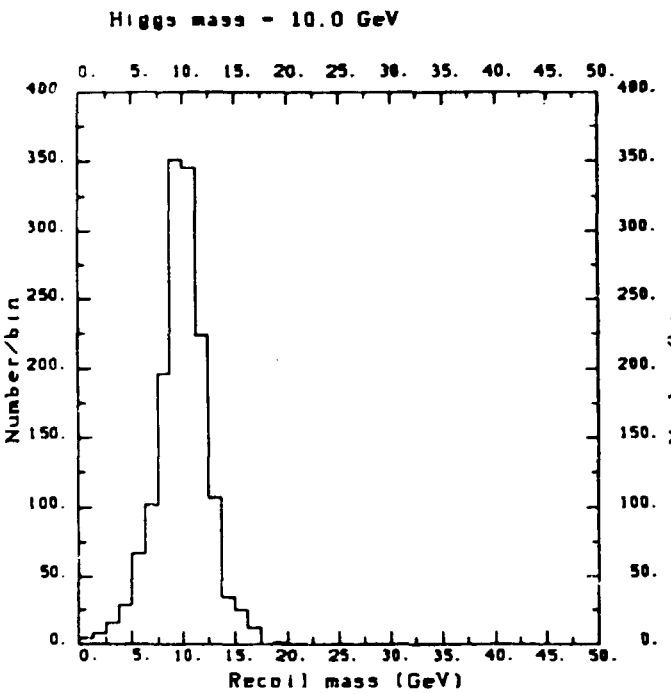

Fig. 10

Histogram of the recoil mass for M_H 10 GeV. In the absence of measurement errors this would be equal to the Higgs boson mass. (Same sample as in Fig. 7.)

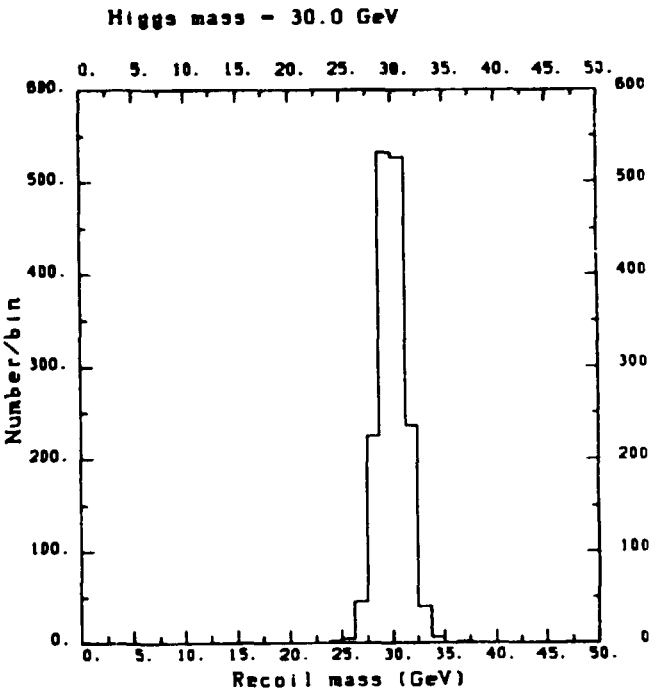

Fig. 11

Same as Fig. 10 for M_H 30 GeV. (Same sample as in Fig. 8.)

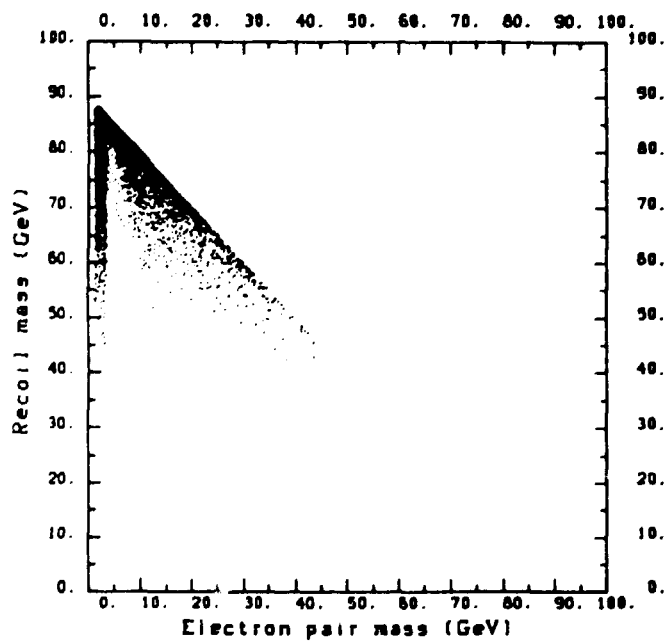

Fig. 12

Scatterplot of the background caused by the decay of $b\bar{b}$ - quarks.

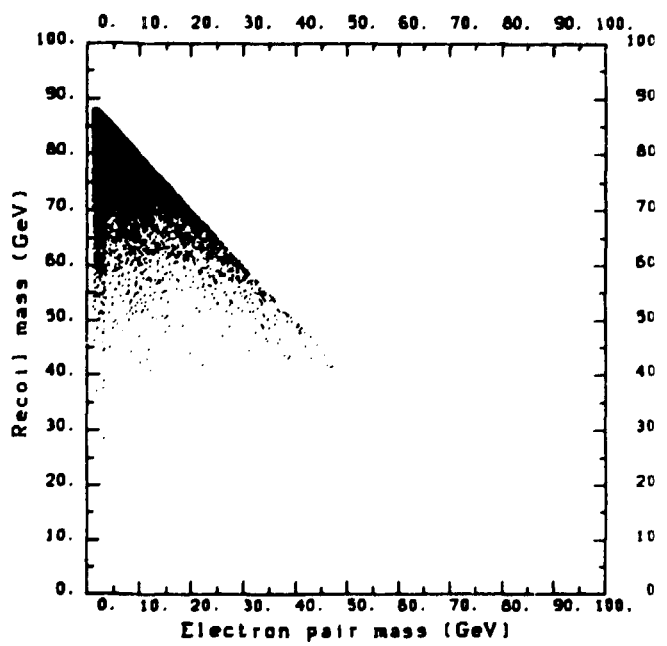

Fig. 13

Scatterplot showing the total background ($c\bar{c}$, $b\bar{b}$ and $t\bar{t}$ in proportions 1 : 1.29 : 1).

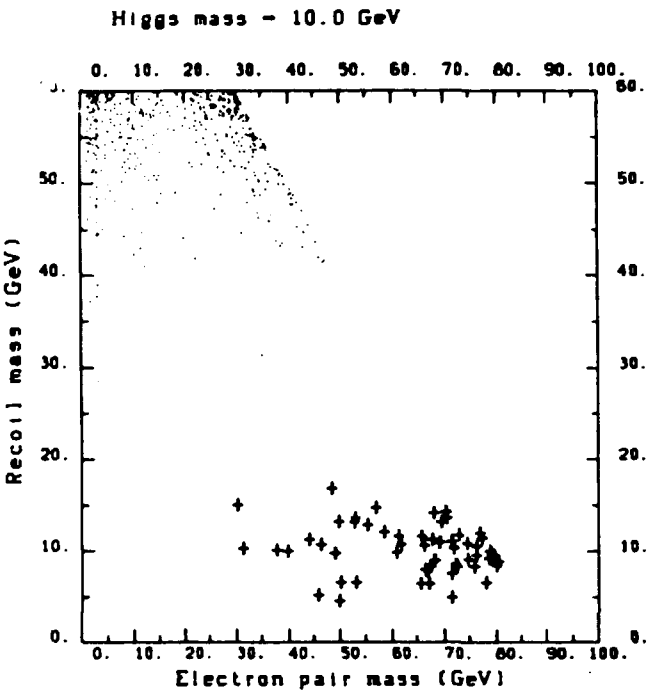

Fig. 14

Scatterplot of background and signal for M_H = 10 GeV. The points from real Higgs boson events are marked with crosses (+).

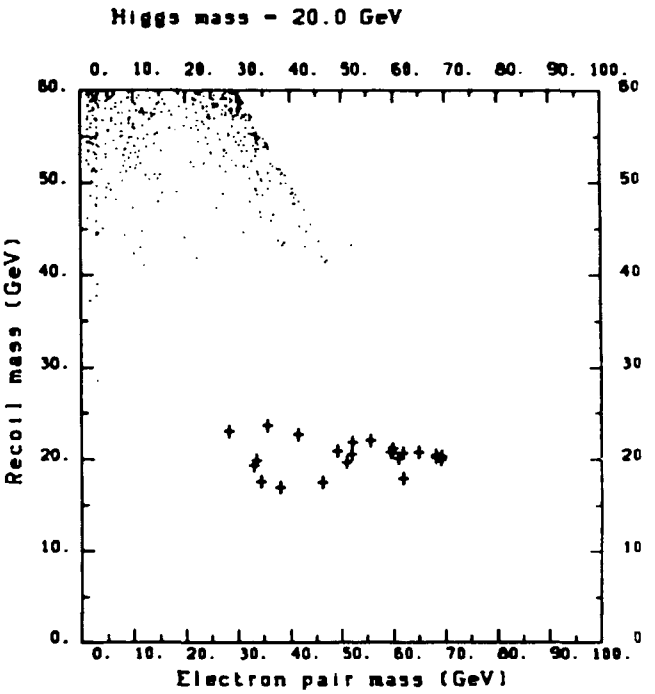

Fig. 15

Same as Fig. 14 for M_H = 20 GeV.

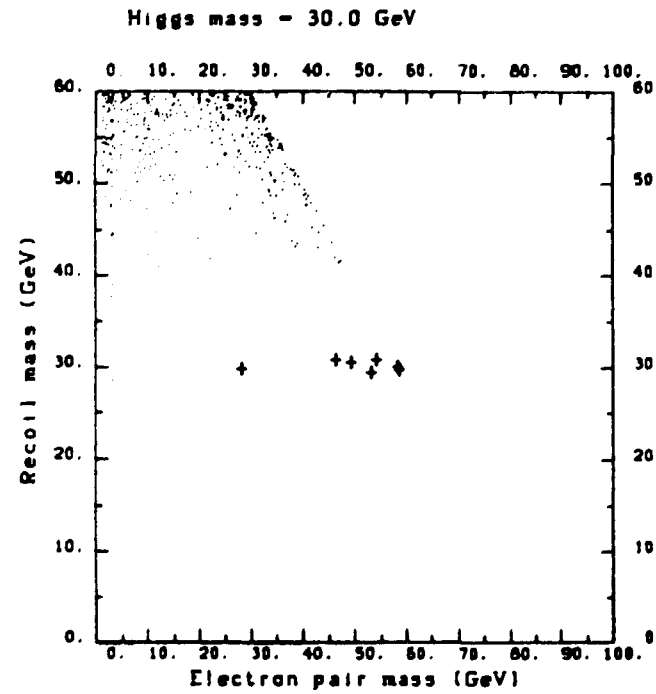

Fig. 16

Same as Fig. 14 for M_H = 30 GeV.

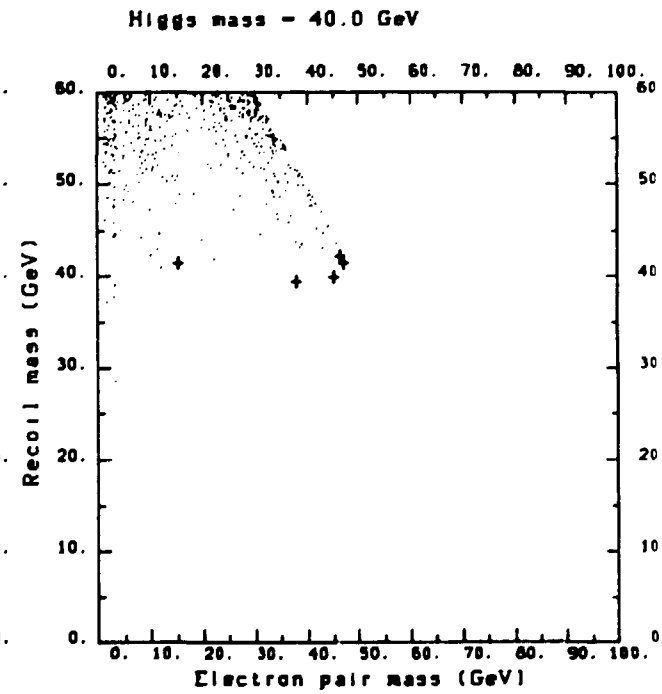

Fig. 17

Same as Fig. 14 for M_H = 40 GeV.

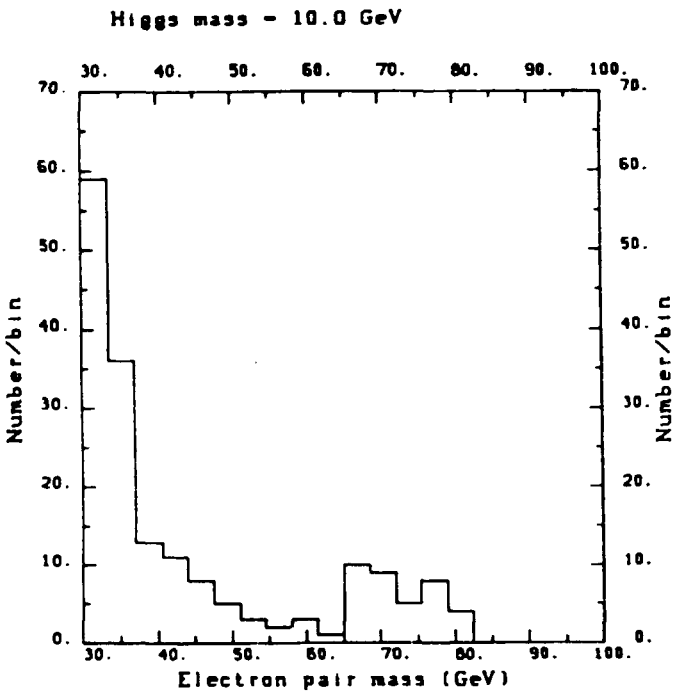

Fig. 18

Histogram of e^+e^- mass of background and signal for M_H = 10 GeV.

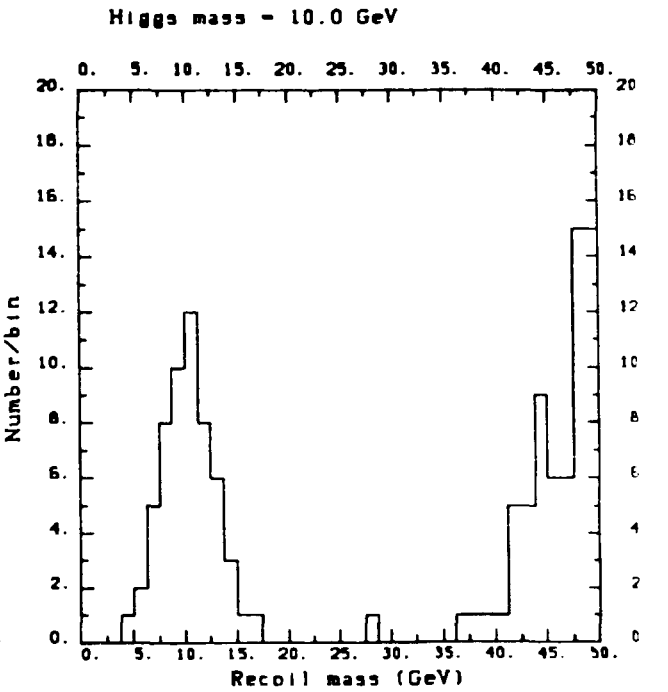

Fig. 19

Histogram of recoil mass of background and signal for M_H = 10 GeV.

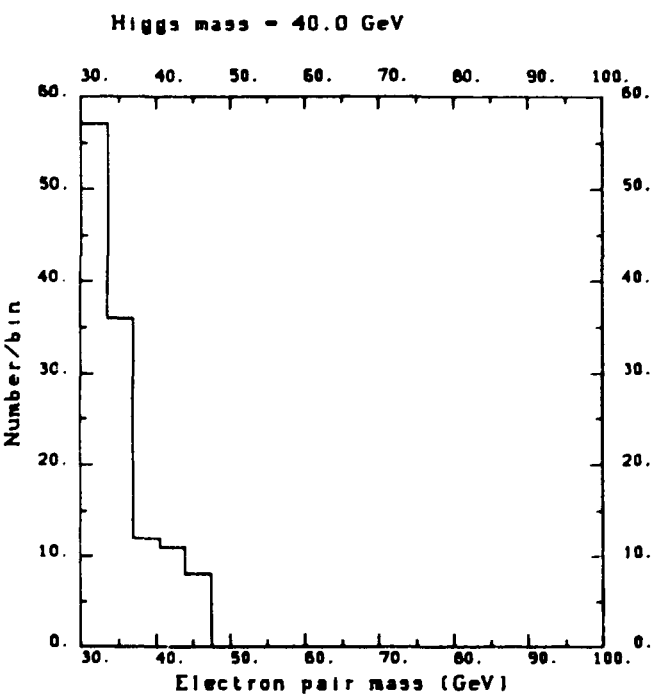

Fig. 20

Same as Fig. 18 for M_H = 40 GeV.

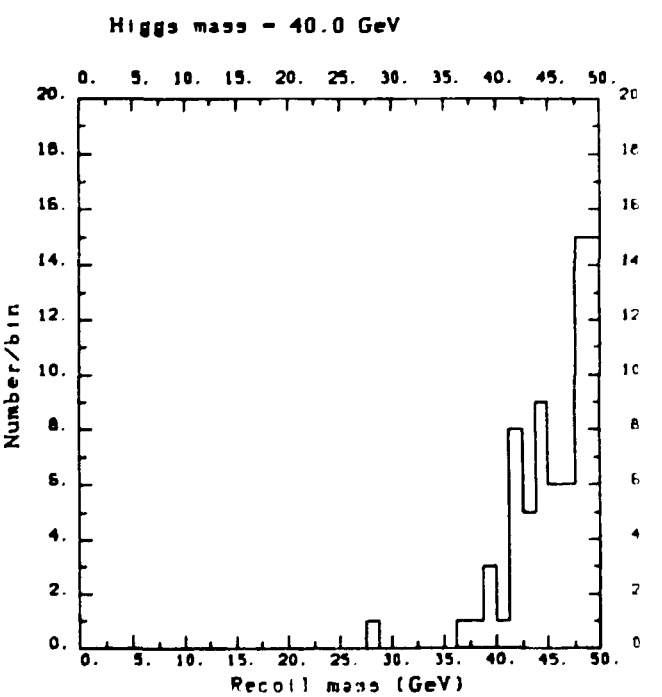

Fig. 21

Same as Fig. 19 for M_H = 40 GeV. (The background is exactly the same as in Fig. 19, permitting an identification of the few boson events merging with the background.)